Carrier Particle Design for Stabilization and Isolation of Drug Nanoparticles

Teresa Tierney,[a] Katalin Bodnár,[a] Åke Rasmuson[a] and Sarah Hudson[a]*

[a]*Synthesis and Solid State Pharmaceutical Centre, Department of Chemical and Environmental Sciences, Materials and Surface Science Institute, University of Limerick, Limerick, Ireland.*

Emails: Teresa.Tierney@ul.ie, Katalin.Bodnar@ul.ie, Ake.Rasmuson@ul.ie, Sarah.Hudson@ul.ie

*Corresponding author: Sarah.Hudson@ul.ie

Abstract

Nanoparticles of poorly water-soluble drugs were prepared in suspension via antisolvent precipitation in order to improve their dissolution behaviour. Insoluble, surface-functionalized, micron-range, clay carrier particles were employed for the dual purpose of stabilizing the nanoparticles in suspended state, and facilitating their unhindered isolation to solid state; often a challenging step in nanoparticle production. The carrier particles, which were functionalized with an optimal level of cationic polymer (protamine), attracted negatively-charged nanoparticles to their surface as a uniform and segregated nanoparticle layer, at drug loadings up to 9% w/w. By using carrier particles to stabilise the nanoparticles on their surface, the traditionally used solubilised nanosuspension stabilisers could be eliminated, thus avoiding time-consuming stabiliser screening tests. The carrier particle system facilitated stabilisation of nanoparticles in suspension, isolation of nanoparticles to the solid state via filtration, and preservation of fast nanoparticle-induced dissolution rates of the dried nanoparticle-carrier composites, indicating preservation of their high surface area during drying. The process was validated with two poorly water-soluble BCS Class II drugs, fenofibrate and mefenamic acid, both of which demonstrated negative surface charge in aqueous suspension.

Keywords

Carrier particles, drug nanoparticles, bioavailability, antisolvent precipitation, filtration, dissolution rate

1. Introduction

Many potential active pharmaceutical ingredient (API) candidates have poor water solubility and slow dissolution rates *in vivo*, leading to limited bioavailability and failure to reach the market [1, 2]. Nano-sizing of pharmaceutical particles to < 1 μm provides an effective means of accelerating their dissolution rate by significantly enhancing their surface area [3, 4]. Such nanoparticles can be prepared in suspension through a variety of crystallization or size reduction approaches, but their isolation from suspension into the dried state is a research area that has been relatively neglected.

Drug nanoparticles in suspended state have a predisposition to physical and chemical instability and have a tendency to grow or aggregate to reduce their free energy. Dissolved additives are generally required to stabilize the nanoparticle size in suspension, requiring rigorous additive-screening approaches. For long term stabilization and for convenience during oral administration, nanoparticles are often isolated into the solid state for incorporation into solid dosage forms such as tablets. Conventional nanoparticle isolation techniques (eg. freeze-drying [5-7], spray-drying [1, 6, 8, 9] and centrifugation [10]) are quite complex processes which can induce nanoparticle aggregation and consequential reduction in dissolution rates compared to suspended nanoparticles.

Some alternative nanoparticle isolation strategies have been proposed in recent years, eg. nanoparticle coating onto water-soluble carriers in a fluidized bed [11], reversible salt- flocculation and filtration [12], and matrix formers for aggregation prevention during spray drying [8]. In 2014, Khan et al. showed that insoluble carrier particles composed of dibasic calcium phosphate could be used to recover nanocrystals of ibuprofen and glibenclamide from suspension by filtration [13]. Filtration is a desirable particle separation technique at industrial scale, but can become problematic when dealing with small micron or nanosized particles. Adsorption of nanoparticles to relatively large carrier materials can facilitate their filtration. The concept of using carrier particles has had widespread application in the preparation of dry-powder inhaler formulations [14-16] and in ordered mixing [17] where sugars have regularly been employed as carrier particles. The report by Khan et al. presented the first and, to our knowledge, only application for carrier mediated isolation of drug nanocrystals from suspension. However, the process was notably limited by a low maximum drug loading of 0.35%, restricting its application to high potency drugs [13]. In addition, prior knowledge of drug-specific, soluble stabilizers was required, which was the focus of an earlier study by the group [10].

This work presents a novel one-step, carrier-mediated method for preparing, stabilizing and isolating fast-dissolving, solid-state drug nanoparticles of poorly water-soluble BCS Class II drugs, fenofibrate

and mefenamic acid. Fenofibrate and mefenamic acid were chosen as model compounds for this study on the basis that nanosizing has been previously shown to enhance their dissolution behaviour [8, 18-22]. Previously, our group prepared and stabilized nanosuspensions of fenofibrate [18], and mefenamic acid [22] by antisolvent precipitation in the presence of dissolved polymer and surfactant-based additives. In both cases, the dissolved stabilizers provided only short-term stabilisation in suspension and were incapable of stabilising the nanoparticles during isolation and drying, causing them to forego their nanoparticle-induced dissolution enhancement. In the present work, the precipitated nanoparticles were captured from suspension and stabilized on the surface of a functionalized clay carrier excipient. Carrier bound nanoparticles were isolated from suspension by filtration, and their fast nanoparticle-induced dissolution rates were preserved during the isolation and drying processes. The previously used optimum additives for each drug system were omitted in the presence of carrier particles, as their function was made redundant. Nanoparticle/carrier composites were prepared with a drug loading of up to 9%, for further use in the final drug formulation.

The carrier (montmorillonite, MMT) is an insoluble, negatively-charged aluminosilicate clay with high ion-exchange capacity. Its surface functionalization agent (protamine, PA) is a positively-charged cationic polymer which can easily adsorb to the clay following an ion-exchange process [23, 24] and attract negatively-charged drug nanoparticles to its surface. Both MMT and PA have FDA approval as inactive ingredients [25] .

2. Material and Methods

2.1. Materials

Fenofibrate (as received, 99.7% purity) and fenofibrate choline salt (crude) were generously gifted from Abbvie Laboratories. Converted fenofibrate (FF) was prepared from the salt form by the procedure outlined in Supplementary Information. Ethanol (99.8%) was purchased from Merck Millipore. Mefenamic acid (MEF, Form I, >98%), N, N-dimethylacetamide (DMA, >99.9%), montmorillonite K10 (MMT), protamine sulphate salt from salmon (PA, amorphous, approx. 5.1 kDa), hydrochloric acid, Tween-80, isopropanol (≥ 99.9%), thionyl chloride (≥ 99.9%) and potassium carbonate (≥ 99%) were purchased from Sigma Aldrich. Potassium dihydrogen phosphate and disodium hydrogen phosphate were purchased from VWR International. TriCor tablets (commercial nanoformulation of FF) were purchased from Abbott. Ponstan capsules (commercial micron

formulation of MEF) were purchased from Chemidex Pharma Ltd. Distilled water was used for sample preparations.

2.2. Functionalization of the Montmorillonite Surface

Protamine sulphate salt was dissolved in water at concentrations ranging from 0.5 – 500 mg/10 mL. Montmorillonite clay (0.4 g – 1 g) was added to the protamine solution, and agitated at 25°C for > 2 hrs. The surface coverage of protamine on montmorillonite was altered by increasing the ratio of protamine to MMT (2 - 1000 mg PA/g MMT) to generate an adsorption isotherm. The saturation limit of protamine on MMT was identified from the adsorption isotherm as the point at which no more protamine adsorbed, and was verified by an increasing protamine concentration in equilibrium solution. PA-MMT samples were equilibrated for > 2 hrs, before vacuum-filtering using Whatman filter paper 50 (2.7 µm pore, 35 mm cross-section). The concentration of protamine remaining in the filtrate was measured by UV-visible spectroscopy (Shimadzu UV-1280) at a wavelength of 200 nm (lower detection limit 0.0025 mg/mL) and served as an indication of the loading of protamine to the MMT. The calibration curve for protamine is shown in Supplementary Information (Fig. S1).

2.3. Zeta Potential Determination

Zeta potential measurments were conducted on a Malvern Zetasizer Nano ZSP system. Zeta potential was determined from the electrophoretic mobility using the Smoluchowski approximation. The precipitated samples (without dilution) were filled into a folded capillary cell and equilibrated at 25 °C for 120 s before measurement. Three measurements were taken per run and each sample was run twice. The average value and the standard deviation between repeated measurements were reported.

*2.4. Synthesis of Nanoparticles and their Loading onto Carrier Particles***.**

Suspended nanoparticles of both fenofibrate (FF) and mefenamic acid (MEF) were generated by antisolvent precipitation. An organic solution of FF in ethanol (1 mL, 50 mg/mL) was quickly introduced by Eppendorf pipet to 10 mL antisolvent containing (a) water, (b) an MMT suspension in water (50 mg/mL, equilibrated for >2 hrs) or (c) a protamine-modified MMT suspension in water (50 mg/mL, 4.6 – 189.9 mg PA/g MMT, equilibrated for >2 hrs). Solutions/suspensions were maintained at 25°C under rapid agitation (800 rpm) throughout the precipitation process. For standard experiments, particles were aged for 1 min before drying. Aging time refers to the time period from precipitation to isolation during which the particles are held in suspension. 1 min aging time before drying was selected since this time was short enough to ensure the nanoparticle size was preserved, but long enough to allow for reproducible and consistent sampling. Exceptions to this aging time

were made for stability testing. Two additional experiments were conducted at (i) 100 mL scale and (ii) where the protamine-modified MMT suspension (50 mg/mL, 4.6 mg PA/g MMT, equilibrated for >2 hrs) was added to the water-precipitated fenofibrate suspension at 20 s after precipitation, and aged for an additional 1 min before drying. FF nanoparticles from preparation (a) were isolated by freeze-drying on a Dura-Dry Microprocessor Control freeze-dryer at <20 Pa for 48 hrs after flash-freezing in liquid nitrogen. Particles from all other preparations were isolated by vacuum-filtration (Mini diaphragm vacuum pump, VP 86) using Whatman filter paper 50 (2.7 µm pore, 35 mm cross section), and washed with 2 mL water. Filter cakes were dried under vacuum (<20 Pa) for 24 hrs and stored at standard ambient temperature before analysis.

Suspended nanoparticles of MEF were prepared and isolated according to the procedure outlined by Bodnar et al. [22] with slight modification. An organic solution of MEF in DMA (0.5 mL, 40 mg/mL, 25 °C) was quickly introduced by Eppendorf pipet to a 9.5 mL aqueous solution of docusate sodium salt (0.53 mg/mL, 5 °C) antisolvent under rapid agitation (1200 rpm). After 1 min aging, free nanoparticles were isolated from suspension by direct filtration with a nylon membrane (0.2 µm). To prepare nanoparticle-carrier composites, MEF was precipitated under the same conditions but with the replacement of the docusate sodium stabilizer in the antisolvent for protamine-modified MMT (42 mg/mL MMT in water, 4.6 mg PA/g MMT). After 1 min aging, particles were vacuum filtered in the same way as the FF-carrier composites.

Nanoparticle attachment to the carrier particles (ie. drug loading) was indirectly monitored by measuring the drug content remaining in the filtrate after filtration (2.7 µm filter pore), and using mass balance to calculate the amount of drug retained by the filter, thus indicating nanoparticle attachment to the carrier. Unattached nanoparticles could pass through the filter to produce a milky filtrate, while carrier-attached nanoparticles could not, resulting in a clear filtrate. An aliquot of the filtrate was diluted by a factor of 10 in methanol and equilibrated for 24 hrs to dissolve any drug particles present before measuring the dissolved drug concentration using a Shimadzu UV-1280 UV-visible spectrophotomer at a wavelength of 289 nm (lower detection limit 0.003 mg/mL). The calibration curve for fenofibrate in a 9:1 methanol:water solution is shown in Supplementary Information (Fig. S2).

Centrifugation was further used to distinguish whether the nanoparticles adsorbed to the PA-modified MMT or if it simply served as a filtration aid to remove the nanoparticles from suspension. Samples containing free FF nanoparticles, a PA-MMT control, and a FF-PA-MMT composite were aged for 0.5 min before centrifuging at a speed of 5000 rpm for 2 min. The supernatant was decanted into a separate vial and the FF content in the supernatant was measured by UV-visible

spectroscopy after dissolving a portion in methanol and leaving to equilibrate for 24 hrs. On knowing the drug content in the supernatant, a mass balance was used to estimate the % of drug which sedimented. This was used as an indicator of the % of drug available which adsorbed to the PA-MMT carrier from suspension.

2.5. Dissolution Testing

The dissolution medium for FF samples consisted of a 0.1 M HCl solution containing 0.4% w/v Tween-80 at 42°C. The dissolution medium for MEF samples consisted of a 0.05 M pH 7.4 phosphate buffer with 0.05% w/v Tween-80 at 37°C. Dissolution tests were carried out in sink conditions by adding a sample (powder or suspension) containing 12.5 mg API to 450 mL dissolution medium (0.0278 mg/mL) under agitation of 400 rpm. TriCor tablets (commercial FF) were ground to a powder by pestle and mortar for 2 min prior to dissolution testing. The powder contained in Ponstan capsules (commercial MEF) was extracted from the capsules for use in dissolution testing. After sample addition, 4 mL aliquots were taken at regular intervals from the bulk solution in preheated (45°C) plastic syringes and filtered through preheated (45°C) PTFE 0.2 µm syringe filters. The dissolved drug concentration was measured by UV-visible spectroscopy (Shimadzu UV-1280) at a wavelength of 289 nm for both FF and MEF (lower detection limit 0.003 mg/mL). The calibration curves for FF and MEF in their respective dissolution media are shown in Supplementary Information (Fig. S3). The dissolution medium was not replaced after each sampling. This work presents the first 10 minutes of dissolution tests, but all dissolution profiles reached approx. 100% dissolved within 5 hours. Dissolution tests were carried out at least in duplicate.

2.6. Particle Size Analysis

Particle size measurements were performed by laser diffraction using a Malvern Mastersizer 3000, with water as the dispersion medium. In cases where the particle size was not stable (Prep (a) in section 2.4), HPMC and SDS were added to the water dispersant at a concentration of 0.038 mg/mL each to minimize variation between consecutive measurements. Precipitated drug suspensions were diluted by a factor of 5 with water prior to their introduction to the measurement vessel. An MMT control was treated by the conditions used during antisolvent precipitation before measuring its particles size. An obscuration rate of 7-10%, a stir rate of 2300 rpm, a 1 min premeasurement delay (including 20 sec with 5% sonication power) were the conditions used during all size measurements. A refractive index of 1.55 and an absorption index of 0.01 were used for FF measurements. A refractive index of 1.55 and an absorption index of 0.1 were used for MMT measurements. Four measurements were taken per run and each sample was run twice. The D_{50} diameter was reported

for each size distribution and averaged across all measurements. The standard deviation of repeated measurements was also reported.

2.7. X-ray Powder Diffraction

X-ray diffraction patterns of the powders were recorded using a PANalytical Empyrean diffractometer in transmission mode, using Ni filtered CuKα radiation (λ=1.54 Å) at 40 kV and 40 mA. The XRD data was recorded in the range of 20.5–23.0 °2θ for FF samples and the range 14.5-16.5 °2θ for MEF samples.

3. Results

3.1. Solid-State Drug-Carrier Composites.

Drug nanoparticles of FF and MEF which were precipitated from a supersaturated solution, captured by a functionalized carrier (PA-MMT), filtered and vacuum dried maintained a dissolution rate which was equivalent to that of the suspended (and stabilized) nanoparticles (300-400 nm) reported previously by our group [18, 22], Fig. 1. The solid-state particles prepared in this way preserved their fast, nanoparticle-induced dissolution rates during isolation and drying, unlike when freeze-drying or direct filtration (0.2 µm) were used, Fig. 1. The PA-MMT carrier alone was able to stabilze the nanoparticle size and surface area (as indicated by dissolution rates) of both FF (9.1% loading) and MEF (4.8% loading) during drying, without the need for the drug-specific dissolved stabilizers which were previously reported for each system [18, 22]. The fast dissolution rates achieved by the dried drug-carrier composites were comparable to or faster than that of their respective dry-powder commercial drug formulations (TriCor $_{[nano]}$ and Ponstan $_{[micron]}$), which were prepared by milling, Fig. 1. Extended dissolution profiles are shown in Supplementary Information (Fig. S4), highlighting that all samples reached approx. 100% dissolved within 5 hrs.

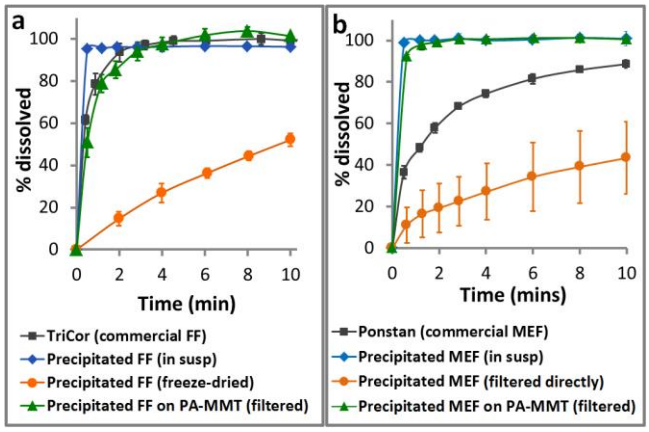

Fig. 1. Dissolution profiles of (a) FF and (b) MEF comparing dissolution profiles of the commercial formulations, and precipitated material in suspension and after drying (1 min aging). Dried particles, in the absence and presence of carrier particles (9.1% FF loading, 4.8% MEF loading) were compared.

Additional tests with the FF system showed that the fast dissolution rate of the dried nanoparticle-carrier composites was maintained when the carrier was added 20 s after, versus before precipitation, when the aging time in suspension was increased from 1 min to 24 hours, or when the process was scaled up from 10 mL to 100 mL, Fig. 2. Furthermore, nanoparticles in the nanoparticle-carrier composites were stable in the dried state over a monitored period of 10 weeks (Fig. S5, Supplementary Information)

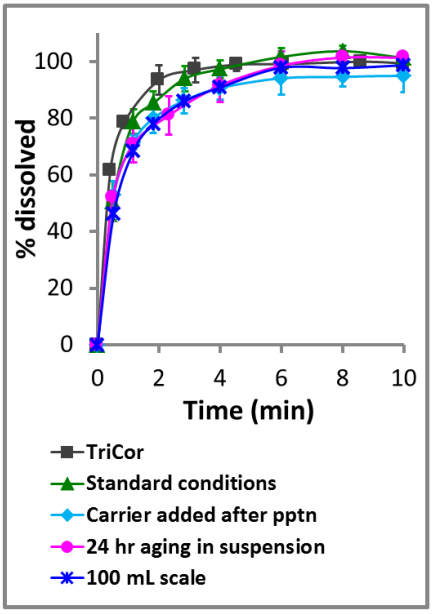

Fig. 2. Dissolution profiles of dried FF composites highlighting the influence of variation from standard conditions (which are: carrier present during precipitation, 1 min aging, 10 mL scale)

Particle sizes of the drug particles in the drug-carrier composites could not be measured directly by laser diffraction due to their attachment to the larger carrier particles. Drug particles were designated as 'nano' particles on the combined basis of their known nanosize in suspension (without carrier particles) and their preserved fast dissolution rates when attached to the carrier particles. Although highly unstable, nanoparticles of FF (D_{50}: 0.75±0.09 µm, Fig. 3) and MEF (D_{50}: 0.84±0.05 µm [22]) existed in suspension at short aging times following their precipitation from water alone.

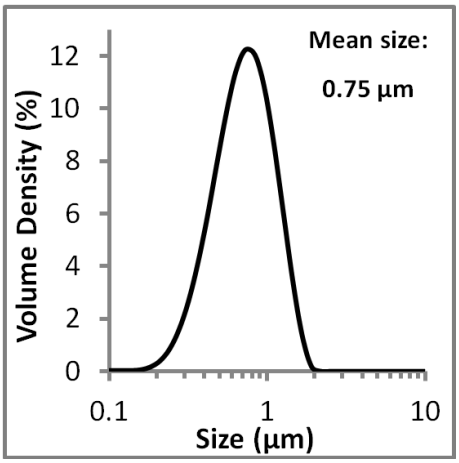

Fig. 3. Particle size distribution of FF precipitated in pure water (no carrier, 1 min aging time)

Similarly, crystallinity of the drug nanoparticles in the drug-carrier composites could not be proven by XRD, solid state NMR or FTIR due to the low drug content compared to the carrier content (9% drug content). Therefore, nanoparticles in the dried nanoparticle-carrier composites were designated as 'crystalline' on the combined basis of their known crystallinity when no carrier was present (Fig. 4), their similar dissolution rates regardless of whether the carrier was present during or added shortly after precipitation (Fig. 2), and based on the diffraction peaks (albeit low intensity) obtained from nanoparticles in the nanoparticle-carrier composites as shown in Fig. 4.

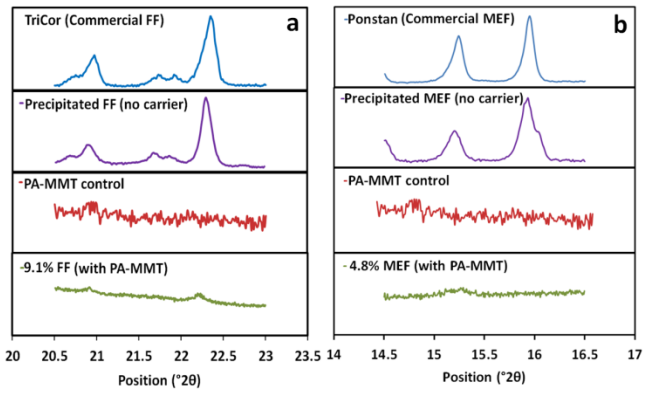

Fig. 4. X-ray diffraction patterns for (a) FF and (b) MEF, comparing commercial formulations and precipitated material after drying (1 min aging time)

3.2. Nanoparticle Attachment to the Carrier.

Attachment of the suspended drug nanoparticles to the PA-MMT carrier (average size: 28.0 ± 1.3 µm, Fig. S6 Supplementary Information) was confirmed by the inability of the carrier-bound FF nanoparticles (0.75 µm) to pass through a 2.7 µm filter, as indicated by a clear FF-free filtrate (containing <0.5% FF). The filtration process was fast, taking < 0.5 min for the mother liquor (11 mL)

to pass through the filter. In comparison, control samples confirmed that >80% of free nanoparticles, precipitated from water or from a PA solution passed through the 2.7 µm filter when no carrier was present (milky filtrate). A schematic of the method used to screen for nanoparticle attachment to the clay is shown in Fig. 5.

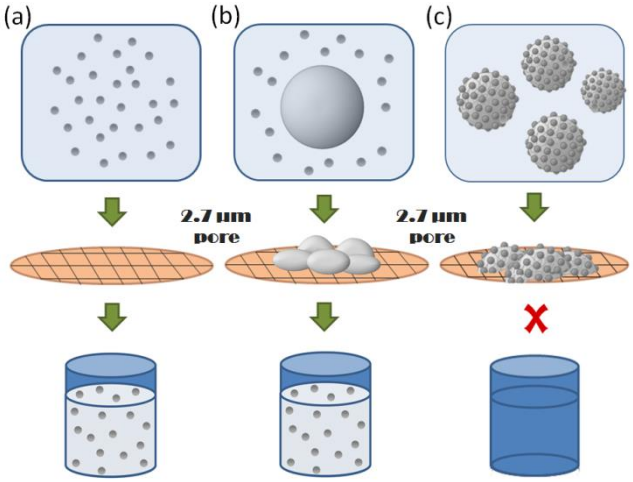

Fig. 5. A filtration test used to indicate nanoparticle adsorption to the carrier. (a) No carrier present, (b) no attachment to the carrier and (c) attachment of nanoparticles to the carrier.

Centrifugation further probed whether the PA-MMT carrier adsorbed the FF nanocrystals to its surface or just served as a filtration aid to separate the nanocrystals from suspension during filtration. Centrifugation allowed the sedimentation ability of the free nanocrystals versus the carrier-attached nanocrystals to be assessed. A control sample of PA-MMT, treated by antisolvent conditions, sedimented during centrifugation. A second control of free FF nanoparticles in suspension only partially sedimented (30%) under the same centrifugation conditions, leaving a milky haze in the supernatant. However, in the presence of the PA-MMT carrier, 98% sedimentation of the FF nanocrystals occurred, giving additional indication of their adsorption to the carrier.

3.3. Role of the PA Modifier.

Free FF nanocrystals (-25.3±0.9 mV, Fig. 6), free MEF nanocrysals (-35.3±1.3 mV [22]) and unmodified MMT carrier particles (-26.9±1.2 mV, Fig. 6) all possess a negative electrical charge in aqueous media. The surface charge of the MMT was modified from negative to positive by the adsorption of protamine, a cationic protein. Fig. 6 shows that the zetapotential of MMT in water changed from -26.9 to -6.1 to +14.8 mV as the surface coating of PA increased from 0 to 4.6 to its saturation value of 200 mg PA/g MMT.

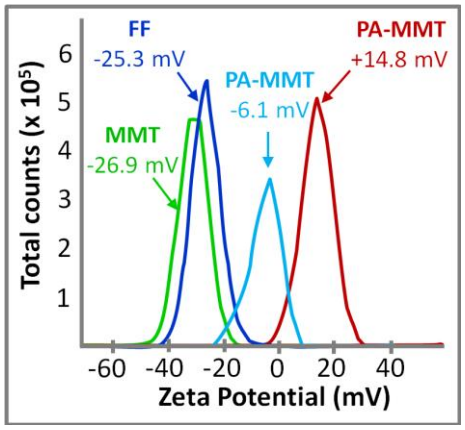

Fig. 6. Zeta potential distributions of aqueous suspensions of FF nanoparticles (-25.3 mV), un-functionalized MMT (-26.9 mV), sparsely PA-functionalized MMT (-6.1 mV, 4.6 mg PA/g MMT) and PA-saturated MMT (+14.8 mV, 200 mg PA/g MMT)

The adsorption isotherm for PA onto MMT followed a non-linear Langmuir-type increase in adsorbed protamine which tended towards its maximum (surface-saturated) value of 200 mg/g MMT, Fig. 7a. The zeta potential of the carrier was dependent on the coating density of protamine on the MMT (mg PA/g MMT), and was easily tuned to between -26.9 mV and +14.8 mV by varying the PA coverage, Fig. 7b. A sparse coating of PA increased the zeta potential significantly.

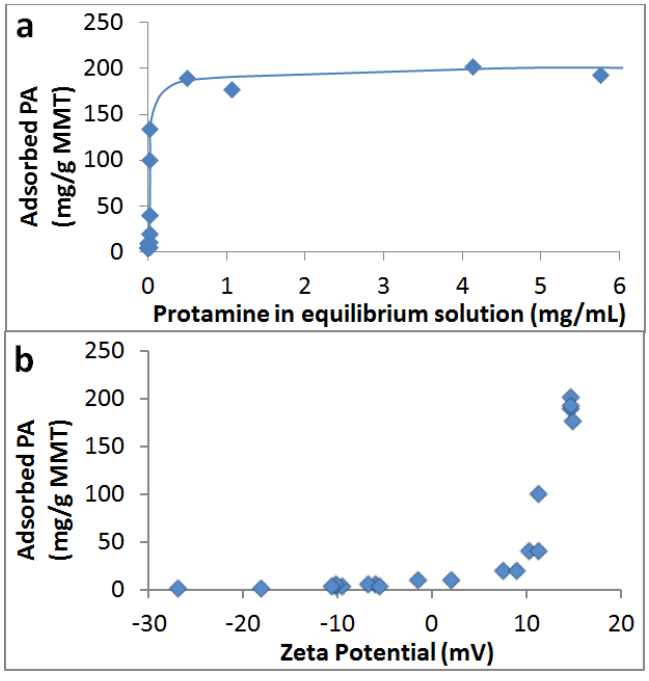

Fig. 7. (a) Adsorption isotherm for PA onto MMT and (b) the effect of adsorbed PA on zeta potential of PA-MMT

Both the nanoparticle loading and the PA loading on the carrier had a bearing on dissolution rates of the dried material, Fig. 8. For the FF system, the maximum drug loading at which nanoparticle-induced fast dissolution rates were preserved in the dried form was 4.8% w/w when no PA-functionalization was present. However, by introducing sparse PA-functionalization and by controlling its coverage on the MMT (4.6 mg/g MMT), the maximum drug loading at which the fast dissolution rate was preserved was increased to 9.1% w/w. Further increase in the PA-coverage on MMT towards its saturation point (200 mg/g MMT) had a negative influence on the dissolution rate, Fig. 8. Therefore, a sparse PA coverage was required for optimum dissolution at high drug loading. For the MEF system, 4.8% w/w was found to be the maximum loading on sparsely PA-functionalised MMT at which the dissolution rate of the dried material was comparable to the nanoparticles in suspension. Dissolution was marginally slower at the higher loading of 9.1% w/w (Fig. S7, Supplementary Information).

For both the FF and MEF systems, the sparse PA coating on the MMT increased the speed of filtration; an important consideration in terms of scalability. Filtration of FF-PA-MMT composites (9.1% loading) was 10 times faster than filtration of FF -MMT composites at 10 mL antisolvent scale (0.5 min vs 5 min), while filtration of MEF-PA-MMT composites (4.8% loading) was 6 times faster than MEF-MMT composites (1.2 min vs 7.5 min).

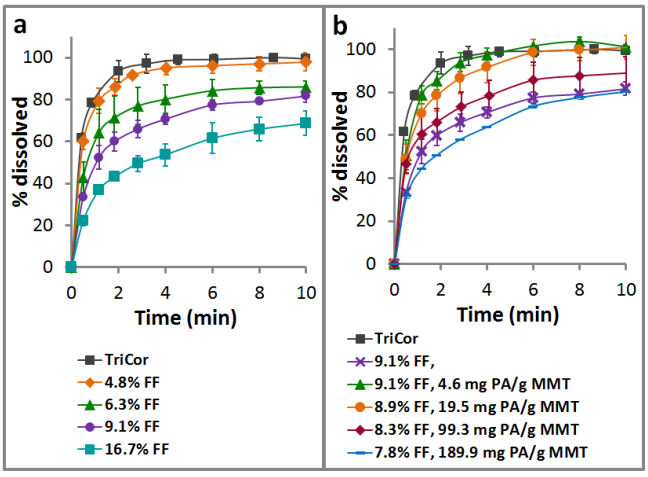

Fig. 8. Dissolution profiles of FF from dried (a) FF-MMT composites at various drug loadings and (b) FF-PA-MMT composites at various PA coverages

4. Discussion

In this work, BCS Class II drugs were formulated into fast-dissolving, solid-state nanoparticle composites using a simple one-step approach. Nanoparticles of fenofibrate and mefenamic acid

were precipitated in suspension in the presence of an insoluble excipient (a functionalized clay carrier) which enabled stabilization, fast filtration, drying, and fast dissolution of the surface-adsorbed nanoparticles. Adsorption of nanoparticles to the carrier was demonstrated both by filtration and centrifugation techniques and the nanoparticles were found to maintain their crystalline form when bound to the carrier. Free nanoparticles of FF and MEF in suspension were previously found to be highly unstable, particularly so in the absence of dissolved stabilizers [18, 22]. This work demonstrated prolonged stabilization of the nanoparticles in suspension (over 24 hrs, Fig. 2) once bound to the functionalized carrier, without the need for the previously reported dissolved stabilizer systems which were identified on the basis of a laborious trial and error stabilizer-screening approach [18, 22]. The prolonged stabilization in the suspended state introduced flexibility to the isolation timeline. The carrier-bound nanoparticles were stable during their isolation (ie. by filtration) and drying stages, as demonstrated by the preservation of fast nanoparticle-induced dissolution rates of the dried material. This result can be compared to nanoparticles isolated by freeze-drying or by direct filtration with a nano-pore filter; two isolation approaches which contributed to reduced dissolution rates, Fig. 1. The nanoparticles in the dried nanoparticle-carrier composites yielded dissolution behaviour equivalent to that of the suspended nanoparticles, and equivalent to or better than those of the commercial formulations (prepared by milling). Furthermore, the use of relatively large carrier particles (~28 μm) facilitated an exchange of more complex, but frequently used nanoparticle isolation methods (eg. spray-drying or freeze-drying) for the simple filtration method. An additional advantage of the carrier approach is the incorporation of the carrier as an excipient at the particle formation step (at drug concentration up to 9%) which bridges the gap between primary and secondary manufacturing, while simultaneously eliminating API-excipient segregation issues.

The surface of montmorillonite clay contains segregated regions of hydrophobicity and charge-induced hydrophilicity. Siloxane (≡Si-O-Si≡) units cover much of its exposed surface, giving the material a hydrophobic nature due to strong bonding interactions between silicon and oxygen atoms [26]. However, isomorphous substitution of selected surface atoms (eg. Si^{4+} by Al^{3+}) provides diffuse regions/patches of permanent (hydrophilic) negative surface charge [23, 27-29], Fig. 9. Negative charges are balanced by adsorption of loosely-bound exchangeable inorganic counterions (eg. Na^{+}, K^{+}), giving the material high ion exchange capacity. In the presence of water, the counterions migrate from the surface and gain a hydration layer which introduces the regional hydrophilic environment between patches of hydrophobic surface [28], Fig. 9.

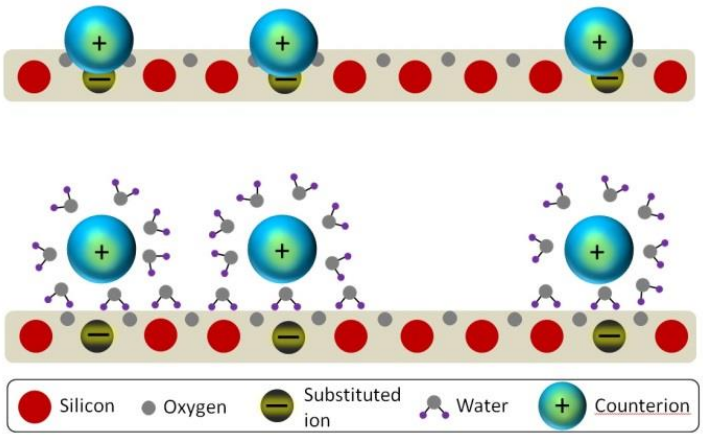

Fig. 9. Graphic description of the MMT surface in the unhydrated (upper) and hydrated (lower) state.

The surface properties of the clay greatly affect the affinity and thus the binding potential and binding mechanism of the drug nanoparticles [29, 30]. In the liquid state, protamine (a cationic polymer) can easily adsorb to the clay following an ion-exchange process [23, 24, 30], providing it with a positively-charged coating. Protamine is rich in arginine which has a basic side chain (pKa of 12.5), giving the material a positive charge in acidic, neutral and even moderately basic environments [31]. The charge reversal of MMT from -26.9 mV to + 14.8 mV upon saturation with protamine confirmed successful deposition of the cationic coating onto the clay, Fig. 6.

Although the negatively-charged drug particles were capable of attaching to the un-functionalized clay (eg. through hydrophobic interactions between methyl/benzene groups and the siloxane surface or through hydrogen bonding with the dangling hydroxyl end groups on MMT [32, 33]), the maximum drug loading at which fast dissolution rates were preserved after drying was low. Due to charge repulsions, the negatively-charged nanoparticles would strictly avoid the negatively charged patches on the clay surface, thus limiting the available favourable adsorption sites, Fig. 10c. At higher drug loadings, nanoparticles may aggregate at the hydrophobic site, resulting in a loss of nanoparticle-induced high surface area and causing a consequential reduction in dissolution rate, Fig. 10d. Surface-modification of the negatively-charged clay with the positively-charged PA was necessary to introduce favourable charged adsorption sites to the clay surface so that the drug could attach both through electrostatic and hydrophobic interaction. It is hypothesized that the increase in the availability of favourable adsorption sites on the MMT surface allowed a homogenous, segregated dispersion of negatively-charged nanoparticles to adsorb to the functionalized carrier, based on their fast dissolution rates after drying, Fig. 10a. However, the surface coverage of PA on the MMT was also influential in preserving the fast dissolution rate. Overcompensation of the

surface with positive charge could induce nanoparticle aggregation surrounding positively charged patches, which is likely the explanation behind the reduced dissolution rates at high PA coating, Fig. 10b. Adsorption of dispersed, fast-dissolving nanoparticles (at >99.5% FF recovery from suspension) was achieved by significantly reducing the surface coverage of protamine molecules (Fig. 8b).

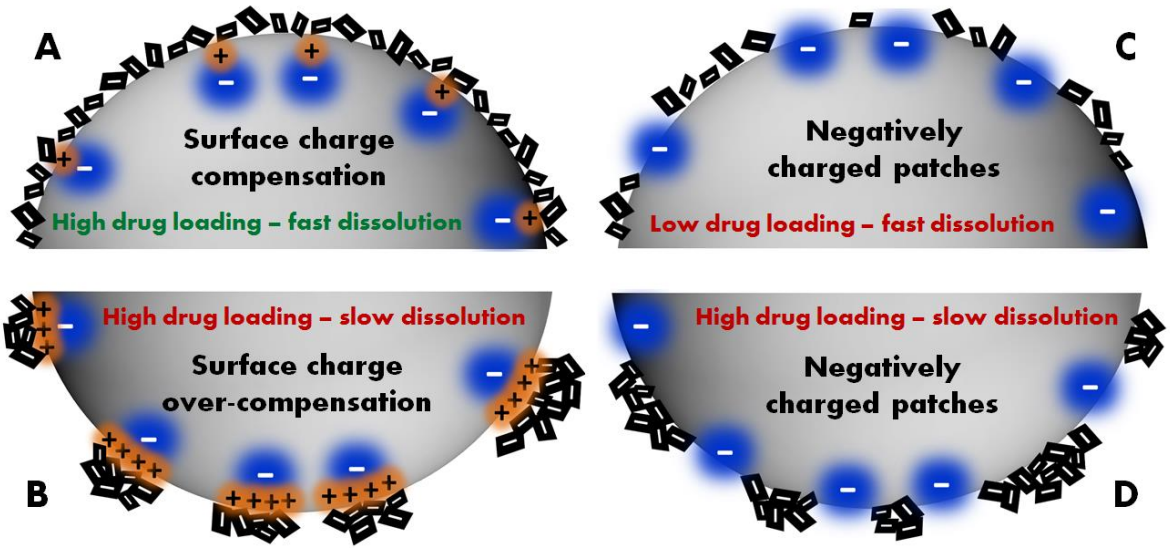

Fig. 10. Mechanistic description of the potential interactions between the negatively charged drug nanoparticles and (A,B) the PA-functionalized and (C,D) the un-functionalized MMT carrier.

MMT has an expanding 3-layer structure with an interlayer spacing of approx. 1-2 nm [32]. Some previous reports have ascribed the adsorption abilities of clays such as montmorillonite for applications in capturing molecules from solution to its large internal surface (eg. in contamination control [30, 34] and drug delivery [24, 32, 35]). In our work however, nanoparticles were first precipitated from solution and their relatively large size permitted adsorption only to the external surfaces of the PA-MMT carrier. Whether the carrier was present during the drug precipitation step or added somewhat later was irrelevant (Fig. 2), as long as nanoparticles were nucleated from solution and the carrier particles were added before too much growth/aggregation occurred.

The carrier-mediated approach to nanoparticle stabilization and isolation outlined in this work was validated by two drugs, but has generic potential in the preparation and isolation of all negatively-charged drug nanoparticles. Furthermore, the same rational may be applied to other combinations of carriers and polymers for tailored application to any drug substance. The antisolvent precipitation technique for nanoparticle preparation, coupled with carrier-mediated isolation by filtration

therefore provides an effective means of formulating particles with enhanced dissolution behaviour, and could have significant application in formulating BCS Class II drugs.

5. Conclusions

This work reports a method by which nanoparticles can be isolated into the dried, solid powder form while retaining dissolution rates which are comparable to or surpass those of the nanoparticles in suspension and currently marketed commercial formulations. Negatively-charged nanoparticles generated in suspension from a supersaturated solution during an antisolvent precipitation method were recovered from suspension using a microparticle carrier system, functionalized with a cationic polymer. The drug nanoparticles were stable on the nanoparticle/microparticle composite (at up to 9% drug loading) in suspension for 24 hours without the requirement for the more traditional nanosuspension stabilizers. The composites were quickly filterable to produce a dried sample with a maintained high drug dissolution rate that stemmed from the nanoparticle size. A more efficient isolation was achieved using a polymer-functionalized carrier, as compared to when an un-functionalized carrier or no carrier was present during filtration. This nanoparticle isolation system was validated by application to particles of two negatively charged drug substances, fenofibrate and mefenamic acid. While success is anticipated for all such drugs, the process has potential to be tailored to an even wider range of drug molecules with modification to the nature of the carrier and its functionalizing agent.

Acknowledgements

This work was supported by the Irish Research Council with additional funding from the Synthesis and Solid State Pharmaceutical Centre and Science Foundation Ireland.

Supplementary Information

Supplementary data (including additional experimental detail) can be found in the online or is available from the authors.

References

1. Zhang, X., J. Guan, R. Ni, L.C. Li, and S. Mao, *Preparation and solidification of redispersible nanosuspensions.* J Pharm Sci, 2014. **103**(7): p. 2166-76.
2. Merisko-Liversidge, E., G.G. Liversidge, and E.R. Cooper, *Nanosizing: a formulation approach for poorly-water-soluble compounds.* European Journal of Pharmaceutical Sciences, 2003. **18**(2): p. 113-120.
3. Kakran, M., L. Li, and R.H. Muller, *Overcoming the Challenge of Poor Drug Solubility.* Pharmaceutical Engineering, 2012. **32**(4).
4. Rawat, N., M.S. Kumar, and N. Mahadevan, *Solubility: Particle Size Reduction is a Promising Approach to Improve the Bioavailability of Lipophilic Drugs.* International Journal of Recent Advances in Pharmaceutical Research, 2011(1): p. 8-18.
5. Matteucci, M.E., M.A. Hotze, K.P. Johnston, and R.O. Williams, *Drug Nanoparticles by Antisolvent Precipitation: Mixing Energy versus Surfactant Stabilization.* Langmuir, 2006. **22**(21): p. 8951-8959.
6. Yue, P., C. Wang, J. Dan, W. Liu, Z. Wu, and M. Yang, *The importance of solidification stress on the redispersibility of solid nanocrystals loaded with harmine.* International Journal of Pharmaceutics, 2015. **480**(1–2): p. 107-115.
7. Van Eerdenbrugh, B., S. Vercruysse, J.A. Martens, J. Vermant, L. Froyen, J. Van Humbeeck, G. Van den Mooter, and P. Augustijns, *Microcrystalline cellulose, a useful alternative for sucrose as a matrix former during freeze-drying of drug nanosuspensions - a case study with itraconazole.* Eur J Pharm Biopharm, 2008. **70**(2): p. 590-6.
8. Dong, Y., W.K. Ng, J. Hu, S. Shen, and R.B.H. Tan, *Clay as a matrix former for spray drying of drug nanosuspensions.* International Journal of Pharmaceutics, 2014. **465**(1/2): p. 83-89.
9. Van Eerdenbrugh, B., L. Froyen, J. Van Humbeeck, J.A. Martens, P. Augustijns, and G. Van den Mooter, *Drying of crystalline drug nanosuspensions—The importance of surface hydrophobicity on dissolution behavior upon redispersion.* European Journal of Pharmaceutical Sciences, 2008. **35**(1–2): p. 127-135.
10. Khan, S., M.d. Matas, J. Zhang, and J. Anwar, *Nanocrystal Preparation: Low-Energy Precipitation Method Revisited.* Crystal Growth & Design, 2013. **13**(7): p. 2766-2777.
11. Basa, S., T. Muniyappan, P. Karatgi, R. Prabhu, and R. Pillai, *Production and in vitro characterization of solid dosage form incorporating drug nanoparticles.* Drug Dev Ind Pharm, 2008. **34**(11): p. 1209-18.
12. Matteucci, M.E., *Highly Supersaturated Aqueous Solutions by Design of Amorphous Pharmaceutical Nanoparticles*. 2007, University of Texas: Austin.
13. Khan, S., M. de Matas, S. Plakkot, and J. Anwar, *Nanocrystal Recovery by Use of Carrier Particles.* Crystal Growth & Design, 2014. **14**(3): p. 1003-1009.
14. Smyth, H.D.C. and A.J. Hickey, *Carriers in drug powder delivery.* American Journal of Drug Delivery, 2012. **3**(2): p. 117-132.
15. Frijlink, H.W. and A.H. De Boer, *Dry powder inhalers for pulmonary drug delivery.* Expert Opin Drug Deliv, 2004. **1**(1): p. 67-86.
16. Wu, S., S. Zellnitz, A. Mercuri, S. Salar-Behzadi, M. Bresciani, and E. Fröhlich, *An in vitro and in silico study of the impact of engineered surface modifications on drug detachment from model carriers.* International Journal of Pharmaceutics, 2016. **513**(1–2): p. 109-117.
17. Yip, C.W. and J.A. Hersey, *Ordered powder mixing.* Nature, 1976. **262**(5565): p. 202-203.
18. Tierney, T.B., Y. Guo, S. Beloshapkin, Å.C. Rasmuson, and S.P. Hudson, *Investigation of the Particle Growth of Fenofibrate following Antisolvent Precipitation and Freeze–Drying.* Crystal Growth & Design, 2015. **15**(11): p. 5213-5222.
19. Hu, J., W.K. Ng, Y. Dong, S. Shen, and R.B.H. Tan, *Continuous and scalable process for water-redispersible nanoformulation of poorly aqueous soluble APIs by antisolvent precipitation and spray-drying.* International Journal of Pharmaceutics, 2011. **404**(1–2): p. 198-204.

20. Ige, P.P., R.K. Baria, and S.G. Gattani, *Fabrication of fenofibrate nanocrystals by probe sonication method for enhancement of dissolution rate and oral bioavailability.* Colloids and Surfaces B: Biointerfaces, 2013. **108**(0): p. 366-373.
21. Tozuka, Y., M. Imono, H. Uchiyama, and H. Takeuchi, *A novel application of α-glucosyl hesperidin for nanoparticle formation of active pharmaceutical ingredients by dry grinding.* European Journal of Pharmaceutics and Biopharmaceutics, 2011. **79**(3): p. 559-565.
22. Bodnar, K., S. Hudson, and A. Rasmuson, *Role of Additives in the Antisolvent Crystallization of Mefenamic Acid Nanocrystals* Submitted: Crystal Growth and Design, 2016.
23. Szabo, T., R. Mitea, H. Leeman, G. Premachandra, and C. Johnston, *Adsorption of protamine and papain proteins on saponite.* Clays and Clay Minerals, 2008. **56**(5): p. 494-504.
24. McGinity, J.W. and J.L. Lach, *In vitro adsorption of various pharmaceutical to montmorillonite.* J Pharm Sci, 1976. **65**(6): p. 896-902.
25. Rowe, R.C., P.J. Sheskey, and M.E. Quinn, *Bentonite*. 6th ed. Handbook of Pharmaceutical Excipients. 2009, London, UK: Pharmaceutical Press.
26. Zhang, X.N. and A.Z. Zhao, *Chemistry of Variable Charge Soils*, ed. T.R. Yu. 1997, Oxford: Oxford University Press. 17-28.
27. Sposito, G., N.T. Skipper, R. Sutton, S.-h. Park, A.K. Soper, and J.A. Greathouse, *Surface geochemistry of the clay minerals.* Proceedings of the National Academy of Sciences, 1999. **96**(7): p. 3358-3364.
28. Liu, X., R. Zhu, J. Ma, F. Ge, Y. Xu, and Y. Liu, *Molecular dynamics simulation study of benzene adsorption to montmorillonite: Influence of the hydration status.* Colloids and Surfaces A: Physicochemical and Engineering Aspects, 2013. **434**: p. 200-206.
29. Chappell, M.A., D.A. Laird, M.L. Thompson, H. Li, B.J. Teppen, V. Aggarwal, C.T. Johnston, and S.A. Boyd, *Influence of smectite hydration and swelling on atrazine sorption behavior.* Environ Sci Technol, 2005. **39**(9): p. 3150-6.
30. Zhu, R., Q. Chen, Q. Zhou, Y. Xi, J. Zhu, and H. He, *Adsorbents based on montmorillonite for contaminant removal from water: A review.* Applied Clay Science, 2016. **123**: p. 239-258.
31. Raman, C.S., P. Martasek, and B. Masters, *Biochemistry and Binding: Activation of Small Molecules*, ed. K.M. Kadish, K.M. Smith, and R. Guilard. Vol. 4. 2000, San Diego: Academic Press. 314.
32. Joshi, G.V., B.D. Kevadiya, H.A. Patel, H.C. Bajaj, and R.V. Jasra, *Montmorillonite as a drug delivery system: Intercalation and in vitro release of timolol maleate.* International Journal of Pharmaceutics, 2009. **374**(1–2): p. 53-57.
33. Wolfe, T.A., *Addition of aliphatic amines to montmorillonite to improve its adsorption capacity for organic pollutants in aqueous solution*. 1981, Iowa State University: Retrospective Theses and Dissertations.
34. Babel, S. and T.A. Kurniawan, *Low-cost adsorbents for heavy metals uptake from contaminated water: a review.* Journal of Hazardous Materials, 2003. **97**(1–3): p. 219-243.
35. Aguzzi, C., P. Cerezo, C. Viseras, and C. Caramella, *Use of clays as drug delivery systems: Possibilities and limitations.* Applied Clay Science, 2007. **36**(1–3): p. 22-36.